Available online at www.sciencedirect.com
ScienceDirect
European Journal of Mechanics B/Fluids 25 (2006) 586–601

Extreme waves, modulational instability and second order theory: wave flume experiments on irregular waves

M. Onorato [a,*], A.R. Osborne [a], M. Serio [a], L. Cavaleri [b], C. Brandini [c], C.T. Stansberg [d]

[a] *Dipartimento di Fisica Generale, Università di Torino, Via P. Giuria, 1, 10125 Torino, Italy*
[b] *ISMAR, 1364 S. Polo, 30125 Venezia, Italy*
[c] *La.M.M.A., Regione Toscana, Via Madonna del Piano, 50019 Sesto Fiorentino, Italy*
[d] *Norwegian Marine Technology Research Institute A.S (MARINTEK), P.O. Box 4125 Valentinlyst, N-7450 Trondheim, Norway*

Received 30 October 2005; accepted 5 January 2006

Available online 12 June 2006

Abstract

Here we discuss the statistical properties of the surface elevation for long crested waves characterized by Jonswap spectra with random phases. Experiments are performed in deep water conditions in one of the largest wave tank facilities in the world. We show that for long-crested waves and for large values of the Benjamin–Feir index, the second order theory is not adequate to describe the tails of the probability density function of wave crests and wave heights. We show that the probability of finding an extreme wave can be underestimated by more than one order of magnitude if second order theory is considered. We explain these observed deviations in terms of the modulational instability mechanism that for large BFI can take place in random wave spectra.

Keywords: Nonlinear waves; Modulational instability; Benjamin–Feir instability; Second order theory

1. Introduction

It is now accepted in the scientific community that large amplitude waves can appear on the surface of the ocean; whether these events are caused by a "fortuitous" linear superposition of different waves with the same phases or are the result of weakly nonlinear interactions is still a debated issue. For linear waves the fundamental work was done by Rice [1] in connection with noise in electronic circuits. Some years later Longuet-Higgins [2] adapted the ideas of Rice to surface gravity waves. He showed that if the wave spectrum is narrow banded and if the phases of the Fourier components of the surface elevation are distributed uniformly (random phases), then the probability distribution of wave heights, crests and troughs is given by the Rayleigh distribution. Corrections to this distribution for wave crests can be obtained if for each wave (free mode), its bound contribution is included. For the narrow-band case this is nothing but describing the surface elevation as a Stokes expansion. The general description of the surface elevation that takes into account bound modes up to second order in wave steepness was given in a seminal paper by Longuet-Higgins [3]. The numerical implementation of the formulas reported in the paper by Longuet-Higgins corresponds to

* Corresponding author.
E-mail address: onorato@ph.unito.it (M. Onorato).

0997-7546/$ – see front matter
doi:10.1016/j.euromechflu.2006.01.002

what today is called the "second order theory". In the narrow-band approximation, for infinite water depth and under the hypothesis that free waves are described by a Gaussian statistics, Tayfun [4] derived a formula for the distribution of wave crests (now known as the Tayfun distribution) which enhances the tail of the Rayleigh distribution, especially if the wave steepness is large. It should be stressed that the Tayfun second order theory still predicts a Rayleigh distribution for wave heights (this is because second order contributions cancel out for wave heights).

In the study of extreme events, it is useful to define the probability that the wave height H or the wave crest η_c assume a value larger than a reference height, H_0. This probability, also known as the survival function $S(H > H_0)$, is given by $1 - P(H \leqslant H_0)$, where P is the cumulative probability function. For the Rayleigh distribution the survival function is given by:

$$S(\xi > \xi_0) = \mathrm{Exp}\left[-2\xi_0^2\right], \tag{1}$$

where $\xi = H/H_s$, with H_s the significant wave height. For the Tayfun distribution, the survival function for wave crests η_c is given by (see also [5]):

$$S(\chi > \chi_0) = \mathrm{Exp}\left[-\frac{8}{(k_0 H_s)^2}\left(\sqrt{1 + 2k_0 H_s \chi_0} - 1\right)^2\right], \tag{2}$$

where now $\chi = \eta_c/H_s$ and k_0 is the dominant wavenumber. It is interesting to note that, according to (2), the survival function depends on the wave steepness. The departure of the Tayfun distribution from the Rayleigh distribution is due to the presence of bound (phase locked) modes and not to the dynamics of free waves. This means that the Stokes wave nonlinearity is accounted for, but the nonlinear interactions among free wave components are not. Using the survival function, it is for example possible to establish that the probability of finding a wave whose height is greater than twice the significant wave height is, using (1), about $1/2980$. The threshold $H/H_s > 2$ is usually selected as a criterion for identifying abnormally high waves (also referred to as freak waves) in a surface elevation time series.

After the pioneering work by Longuet-Higgins [2], the validity of the Rayleigh distribution for wave heights has been widely investigated. The distribution (1) was found to agree well with many field observations [6] even though the frequency spectrum was not always so narrow and the steepness was not as small as required by the theory. During the last 30 years, many empirical distribution functions have been proposed to better fit the data. Forristall [7] analyzed data recorded during hurricanes in the Gulf of Mexico and obtained better agreement with a two parameter Weibull distribution. According to his analysis, the Rayleigh distribution was over-predicting the experimental data. Some years later Longuet-Higgins [8] re-examined the same data and showed that the Rayleigh distribution fitted equally well the data, provided that the value of the root mean square wave amplitude is suitably modified by introducing a finite spectral bandwidth (see also [9]).

In recent years particular attention has been given to understanding the mechanism of formation of freak waves and their influence on the tail of the probability density function of wave heights. A number of physical mechanisms have been identified: linear superposition, the wave-current interaction ([10] and [11]) and the modulational instability ([12,13], see for example [14] for a recent review on different mechanisms). Nevertheless, it should be stated that, except for some recent papers [15–17], not much progress has been made concerning the resulting statistical properties of the surface elevation. More in particular, the relation between the various sea states and the probability density function has not been clearly identified.

Limiting the study to one-dimensional propagation, Onorato et al. [18] have performed numerical simulations of the Nonlinear Schrödinger and Dysthe equations with initial conditions provided by Jonswap spectra with different values of the enhancement factor γ and of the Phillips constant α (γ is related to the spectral band-width and the wave steepness; α is responsible for the energy content of the surface elevation and therefore contributes to the wave steepness). One interesting result is that the probability density function substantially depends on these two parameters α and γ. For small values of α and γ the Rayleigh distribution approximates the data rather well, but for large values of α and γ the Rayleigh distribution clearly underestimates the tail of the probability density function (see Fig. 6(b) in [18]). For example, using the Dysthe equation, with a Jonswap spectrum with $\gamma = 6$ and $\alpha = 0.0081$ as initial conditions, the probability of recording a freak wave (defined as a wave whose height is at least twice the corresponding significant wave height) is $1/630$, almost 5 times greater than the one predicted by the Rayleigh distribution! Strong departure from the Rayleigh distribution was also observed numerically [19,20], using the Higher Order Spectral method [21] for solving the Euler equations for surface gravity waves. This departure from the Rayleigh distribution was attributed to the Benjamin–Feir instability mechanism that, provided the spectrum is sufficiently narrow and the steepness is sufficiently large, can take place also in random waves [22].

Following the ideas developed in [22] and successively in [23], Onorato et al. [24] studied the instability of a narrow banded approximation of a Jonswap spectrum, identifying the region of instability of the spectrum in the α–γ plane. They found that, as a result of the modulational instability, oscillating coherent structures (these structures are particular "breather" solutions of the NLS equation, see [25] and [26]) may be excited also from random spectra. More recently Janssen [15] discovered that the region of instability predicted using the theory developed in [22] is not completely consistent with direct simulations of the NLS and Zakharov equations. He therefore developed a kinetic equation that takes into account quasi-resonant interactions and demonstrated good agreement between theory and direct numerical simulations; moreover he was also able to compute from the theory some statistical properties of the surface elevation such as, for example, the kurtosis. He found that, if the ratio between the steepness and the spectral bandwidth is large (the ratio is often referred to as the Benjamin–Feir Index (BFI), see also [27]), the Gaussian distribution underestimates the tails of the probability density function for the surface elevation. Note that in his analysis the statistics was computed only on free waves, the Stokes contribution was not included. Even though it was not mentioned in the paper, we expect that in such conditions also the survival function for wave heights should be far from being well described by (1). One of the major results in [15], that confirms previous results from numerical simulations in [18] and [27], is therefore that the statistical properties of the surface elevation for free waves strongly depend on the BFI (therefore also on the spectral shape, see Section 2). This conclusion, limited to deep water waves and to one-dimensional propagation, has been reached from simplified models, without including any mechanism of dissipation such as wave breaking.

Concerning random wave experiments in wave tank facilities, in the past 15 years it has been recognized that at about 15–20 wavelengths from the wave maker extreme individual wave heights in random records may appear more frequently than predicted by the Rayleigh distribution (see for example [28] and references therein). The increase of the kurtosis observed along the wave tank in [29] was interpreted as a higher-order effect, attributed to the modulational instability. Nevertheless, to the knowledge of the authors, even though Jonswap spectra are common runs in wave flumes for many different applications, there has not been any systematic experimental study devoted to understanding the relation between the BFI and the probability density function of wave heights. In this paper we discuss some experimental results that we have obtained in a large facility at Marintek, Trondheim (Norway). Our main goal in this paper is to give some experimental support to the numerical and theoretical work performed in recent years that suggests the idea that the modulational instability can be responsible for the formation of large amplitude waves. Note that, as previously discussed, it is well known (see for example [30]) that the statistical properties of the wave amplitude can have deviations from Gaussian behavior due to the Stokes contribution (bound waves). In this paper however we are mainly interested in investigating the deviations from Gaussianity as a result of the interactions between free waves and in particular those arising from the modulational instability.

Herein we will often refer to the NLS equation. The description of the NLS equation in our manuscript helps us to introduce in a simple and didactic way a number of concepts such as the Benjamin–Feir index or "unstable modes". For almost a century water waves have been often characterized basically by their linear dispersion relation; this was the result of the solution of the linearized Euler equations for water waves. In the weakly nonlinear approximation, the NLS appears naturally as the leading order equation. It contains very nice physical and mathematical properties that can be used to understand more complex physical situations just as the linear dispersion relation has helped (and still does help) to understand many physical properties of water waves. We are not using the NLS as a model equation to reproduce our experimental data; we are instead only using the concept of the BFI as an initial indicator of nonlinearity in our data. Our aim is to show from experimental data that the statistical properties of the surface elevation can substantially deviate from the Gaussian behavior whenever the Benjami–Feir index is large enough.

The paper is organized as follows: Section 2 contains a derivation of the BFI; with respect to previous works we extend the definition of the BFI to arbitrary depth. Sections 3 and 4 are devoted to the description of the experiment and of the results. Discussions and conclusions are reported in Section 5. We mention that some of the results concerning the extreme statistics on the same experimental data have already been discussed as brief communications in [31] and [32]. We here consider a direct comparison between our experimental data and results from Tayfun and second order theory. Our results are consistent with recent numerical simulations of higher order NLS equation in the case of long-crested initial conditions performed in [5]. We give a complete description of the experiment including the evolution of statistical quantities such as significant wave height, wave steepness and wave spectra along the tank.

2. The Benjamin–Feir index and its relation to the Jonswap spectrum

The Benjamin–Feir index in the context of freak waves has been introduced formally for random waves in [15] (see also [27]). It can be obtained in two different ways: The first more laborious one consists in following the approach by Alber [22], i.e. one starts from the Nonlinear Schrödinger equation, derives a kinetic equation for inhomogeneous surface elevation, performs a linear stability analysis of an homogeneous random spectrum and obtains its condition of stability (see [15] for details). The resulting condition simply states that a spectrum is stable if the BFI is less than one. A simpler approach, the one that will be presented here, proposed in [27], is based on dimensional arguments (note that in [27] the square of the BFI was considered and was referred to as an Ursell number). We will start from the simplest weakly nonlinear model that describes the evolution of free waves, derived from the Zakharov equation under the narrow-band approximation (see [33]). The dimensional NLS equation in arbitrary depth, in a frame of reference moving with the group velocity, has the following form:

$$\frac{\partial A}{\partial t} + \mathrm{i}\sigma \frac{1}{8}\frac{\omega_0}{k_0^2}\frac{\partial^2 A}{\partial x^2} + \mathrm{i}\beta \frac{1}{2}\omega_0 k_0^2 |A|^2 A = 0, \tag{3}$$

where A is the complex wave envelope, k_0 is the carrier wave number and ω_0 is the respective angular frequency. σ and β are functions of the product $k_0 h$, with h the water depth, and both tend to 1 as $k_0 h \to \infty$. The analytical forms of σ and β can be found in the book of Mei [34] and are also reported in the appendix. The next step consists in adimensionalizing equation (3) in the following way: $A' = A/a_0$, $x' = x\Delta K$ and $t' = t(\Delta K/k_0)^2 \sigma\omega_0/8$, where ΔK represents a typical spectral band-width, a_0 a typical wave amplitude. Eq. (3) reduces to:

$$\frac{\partial A}{\partial t} + \mathrm{i}\frac{\partial^2 A}{\partial x^2} + \mathrm{i}\left(\frac{2\epsilon}{\Delta K/k_0}\right)^2 \frac{\beta}{\sigma}|A|^2 A = 0, \tag{4}$$

where primes have been omitted. $\epsilon = a_0 k_0$ is a measure of the wave steepness. We define the Benjamin–Feir index as the square root of the coefficient that multiplies the nonlinear term:

$$BFI = \frac{2\epsilon}{\Delta K/k_0}\sqrt{\frac{|\beta|}{\sigma}}. \tag{5}$$

The term $\sqrt{|\beta|/\sigma}$ on the right hand side includes the influence of the water depth. The effect of this last term on the BFI as a function of $k_0 h$ is shown in Fig. 1. As the water depth increases the function tends to one and goes to zero for shallower water. For values of $k_0 h$ smaller than about 1.36, the coefficient in front of the nonlinear term in the NLS changes sign and the equation becomes stable with respect to side band perturbations. As the BFI increases the nonlinearity increases; therefore we expect that the number of freak waves increases. Note that this result was first obtained numerically with numerical simulations of the NLS equation in [27].

Normally one measures time series rather than space series; therefore, for the computation of the BFI from experimental data, the term in the BFI for infinite water depth $\Delta K/k_0$ should be replaced by $2\Delta f/f_0$ where f_0 is the

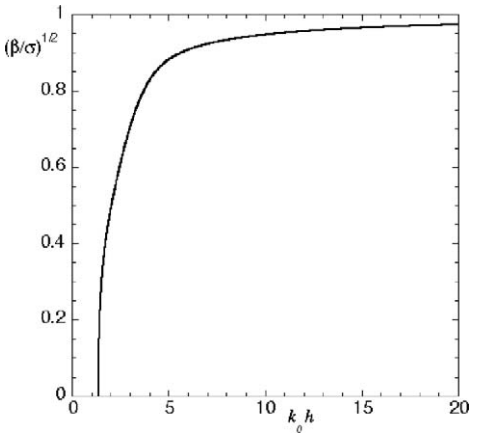

Fig. 1. Effect of finite water depth on the BFI. Note that the curve has been plotted for values larger than 1.36 for which β is positive.

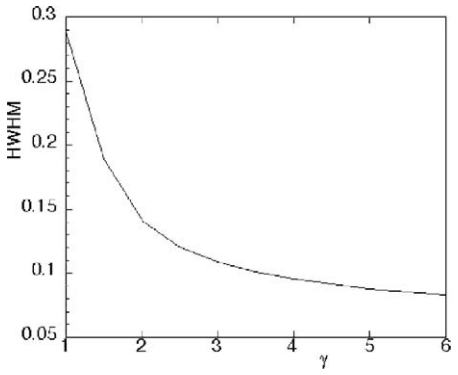

Fig. 2. Half-width at half-maximum as a function of the enhancement parameter γ.

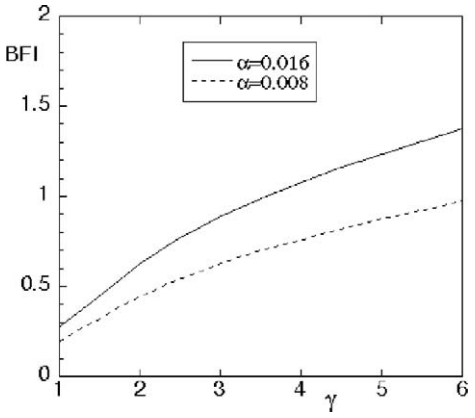

Fig. 3. BFI as a function of the enhancement parameter γ for $\alpha = 0.008$ and $\alpha = 0.016$.

frequency at the spectral peak and Δf the spectral band-width. Therefore, given a time series, we will estimate the BFI in the following way: the wave spectrum is computed; the half-width at half maximum provides an estimate of the spectral-band width, Δf. Methods such as those based on the quality factor (see for example [23]) could also be used for the calculation of the spectral width. Nevertheless for our purposes, we find our simple and straightforward method to be satisfactory. Using the linear dispersion relation, the peak frequency is converted into the peak wavenumber and the steepness is then computed as $\epsilon = k_0 H_s/2$, where H_s is the significant wave height computed as 4 times the standard deviation of the time series. We have applied this methodology in order to establish the relation between the BFI and the Jonswap spectrum (see e.g. [35]):

$$P(f) = \frac{\alpha g^2}{(2\pi)^4 f^5} \exp\left[-\frac{5}{4}\left(\frac{f_0}{f}\right)^4\right] \gamma^{\exp[-(f-f_0)^2/(2\sigma_0^2 f_0^2)]}, \tag{6}$$

where $\sigma_0 = 0.07$ if $f \leqslant f_0$ and $\sigma_0 = 0.09$ if $f > f_0$, g is gravity acceleration, α is the Phillips constant and γ is the enhancement parameter. We mention that here there is no attempt to parameterize wind wave spectra. Our particular use of the Jonswap spectrum is just motivated by the fact that the spectrum is well known and recognized in the field of wind waves; other spectral shapes described for example in [36] could have just as easily been used. Our goal here is to study the statistical properties of surface elevation as we change the ratio of the wave steepness to the spectral band-width. We have accomplished this by suitably changing in a consistent way (see next section) the parameters α and γ in the Jonswap spectrum.

As it is shown for example in [36], the steepness is a function of both γ and α: an increase of any of these two parameters results in an increase of the steepness. Moreover, the spectral band-width is also a function of γ, as can be seen in Fig. 2 where we show the influence of the parameter γ on the half-width at half-maximum (HWHM). As an example and without any attempt at parameterizing wind wave spectra, in Fig. 3 we now show the BFI as a function of γ for $\alpha = 0.008$ and $\alpha = 0.016$ (here we have considered the case of infinite water depth). We note that for α constant, larger values of γ imply a larger value of the Benjamin–Feir index. The Phillips constant α is strictly related to the wave energy, therefore to the wave steepness, $\alpha \sim \epsilon^2$. If we double the value of α with γ constant the steepness increases by a factor of $\sqrt{2}$ and so does the BFI (the spectral band-width remains practically unchanged).

Here we mention that the BFI and its quantitative use for studying the stability of a wave train is today defined in a unique way only for the case of a perturbed Stokes wave: a carrier wave with two small side bands. For random waves, different estimation of steepness and spectral bandwidth can lead to different numerical values of the BFI (see [37]).

3. Description of the experiments

The experiment was carried out in the long wave flume at Marintek (see [38] for details on the facility). The length of the tank is 270 m and its width is 10.5 m. The depth of the tank is 10 meters for the first 85 meters, then 5 meters for the rest of the flume. The effect of the jump from 10 to 5 meters is insignificant for the waves of 1.5 seconds considered here: It can be easily seen from linear theory that the particle velocities at 5 meter depth are essentially

zero. A horizontally double-hinged flap type wave-maker located at one end of the tank was used to generate the waves. The distribution of signal frequencies to the upper and lower flap is automatically applied by control software. All flap motion is computer controlled by using pre-generated digital control signals stored in files. A sloping beach is located at the far end of the tank opposite the wave maker. After half an hour of an irregular wave run with peak period of 1.5 seconds, the wave reflection was estimated to be less than 5%. The wave surface elevation was measured simultaneously by 19 probes placed at different locations along the flume. Twin-wire conductance measuring probes were used; these have excellent calibration characteristics. Each wire was 0.3 mm in diameter, separated 10 mm from its twin in the direction perpendicular to the main axis of the tank. A view of the flume with the location of the probes is shown in Fig. 4. Preliminary simulations with the one-dimensional NLS equation were performed in order to estimate the spatial scales needed for the modulational instability to develop in a random spectrum. Note that an estimation of these scales based on the dispersion relation from small perturbation theory of plane wave solutions is not adequate because in a random Jonswap spectrum the perturbations are never small! For steepness of around 0.1, we estimated from numerical simulations that the instability would take place at around 20–25 wavelengths, i.e. for 1.5 seconds waves at around 60–75 meters from the wave maker. This is why a larger number of probes were placed in that region. Lateral probes were also placed at 75 and 160 meters in order to verify the quality of the long-crested waves generated at the wave maker. The sampling frequency for each probe was 40 Hz. Jonswap random wave signals where synthesized as sums of independent harmonic components, by means of the inverse Fast Fourier Transform of complex random Fourier amplitudes. These were prepared according to the "random realization approach" by using random spectral amplitudes as well as random phases. Three different Jonswap spectra with different values of α and γ have been investigated. Our selection of α and γ is consistent with Figs. 5(c) and 5(f) in [36], where α and γ are plotted as a function of the steepness for the Jonswap experiment. All of the spectra were characterized by a peak period of 1.5 seconds. In Table 1 we report the parameters that characterized each Jonswap spectrum. The value of $\sqrt{\beta/\sigma}$ in the BFI was estimated to be 0.95 at the wave maker. In order to have sufficiently good statistics, a large number of waves was recorded. Note that the large amount of data is of fundamental importance for the convergence of the tail of the probability density function for wave heights. Therefore for each type of spectrum, 5 different realizations with different sets of random phases have been performed. The duration of each realization was 32 minutes. The total number of wave heights (counting both up-crossing and down-crossing) recorded for each spectral shape at each probe was about 12 800 waves. In our analysis we have removed the first 200 seconds of the records for each realization. This lapse of time was calculated as the approximate time needed for the wave of twice the peak-frequency to reach the last probe.

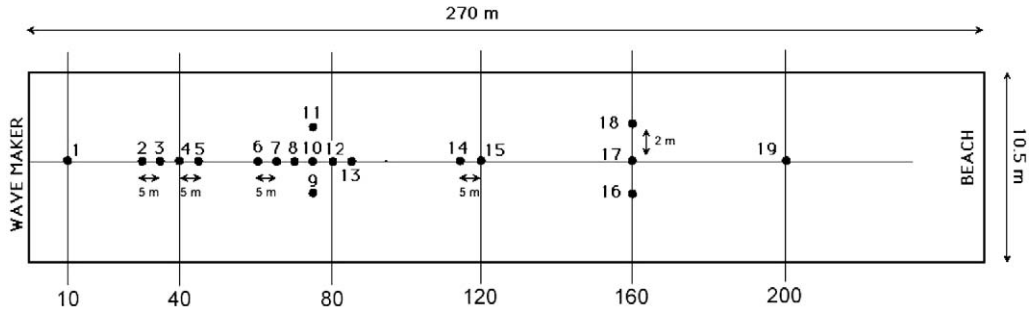

Fig. 4. Sketch of the wave tank facility at Marintek and location of wave probes.

Table 1
Parameters of the three different experiments performed at Marintek

γ	$H_s(m)$	$\epsilon = k_0 H_s/2$	$\Delta f/f_0$	BFI
1	0.11	0.1	0.28	0.2
3.3	0.14	0.13	0.09	0.9
6	0.16	0.15	0.08	1.2

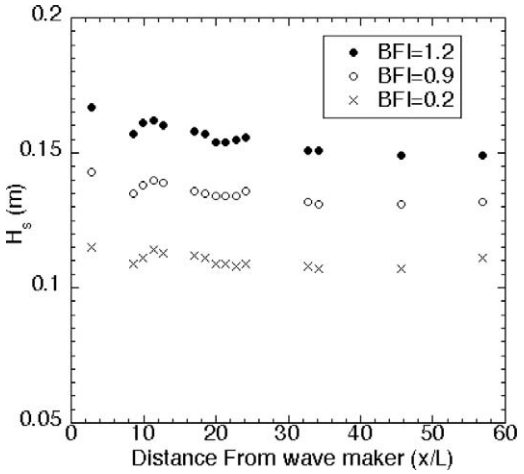

Fig. 5. Evolution of the significant wave height as a function of nondimensional fetch: BFI = 0.2, crosses; BFI = 0.9, empty circles; BFI = 1.2 full circles (see Table 1). The horizontal axis has been nondimensionalized with the characteristic wavelength computed using the linear dispersion relation.

4. Experimental results

4.1. Significant wave height, wave spectra and wave steepness

Before describing the statistical properties that are related to the extreme events, we give some details on standard properties such as the significant wave height, steepness and wave spectra along the tank. In Fig. 5 we show the significant wave height as a function of nondimensional fetch (distance from the wave maker). As we can see from the figure, the significant wave height decreases slightly for BFI = 1.2 and BFI = 0.9 along the tank and it is essentially constant for BFI = 0.2. We mention that the present experiment was not designed to study wave breaking and no quantitative measures of wave breaking are available; moreover the wave tank is 270 meters long and it was not easy to estimate visually the number of breakers in the tank. Nevertheless we can confidently state that wave breaking was observed more frequently for larger BFI. This is consistent with Fig. 5 where a decrease of significant wave height is observed for larger BFI. In Figs. 6, 7 and 8, we show the evolution of wave spectra in logarithmic coordinates for three different values of $x/L = 2.8$, $x/L = 21.2$ and $x/L = 56.9$. Here L is the dominant wavelength, $L = 3.51$ m, which corresponds to the peak period at the first probe. In the log-log representation we can see that in all three cases the level of the tail of the spectrum is reduced as the waves propagate along the tank. Moreover, especially for BFI = 1.2 the peak of the spectrum is also substantially reduced already at $x/L = 21.2$ and a downshift is also evident. This result is consistent with recent numerical simulations in [39] and [15], where a change of the spectrum is already seen on the scale of the Benjamin–Feir instability. In Fig. 9 we show the evolution of the steepness ϵ computed as $\epsilon = H_s k_0/2$ where the k_0 is the dominant wavenumber computed using the linear dispersion relation using the dominant frequency f_0. Again we see a decay of the steepness especially for BFI = 1.2 and BFI = 0.9. This is primarily due to two reasons: H_s is decreasing and a downshift of the spectral peak is also observed for large BFI.

4.2. Extreme statistics: kurtosis and rogue wave density

We now study the behavior of some statistical quantities that can give an indication about the presence of extreme events in the time series. In [31] and [32] the behavior of the kurtosis, which is a measure of the importance of the tails of the probability density function of wave heights, was described. It was shown that for the two large BFI cases, large deviations from the Gaussian value have been observed after some wavelengths from the wave maker. In [32] it was also shown with the use of numerical simulations of the Dysthe equation and with a band pass filtering of the data around the peak that the departure from the Gaussian behavior was mainly due nonlinear interactions around the peak of the spectrum Note also that those results are supported by numerical simulations of the Zakharov equation (see Fig. 7 or 12 in [15]), where only free waves are simulated and a clear departure from the Gaussian statistics is

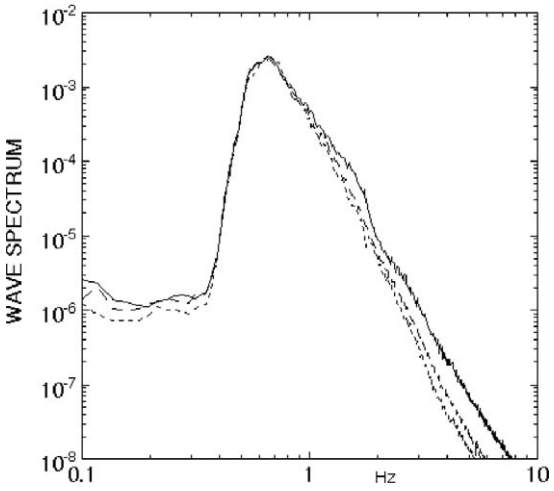

Fig. 6. Wave spectra for BFI = 0.2 at $x/L = 2.8$ (solid line), $x/L = 21.2$ (dashed line) and $x/L = 56.9$ (dotted line).

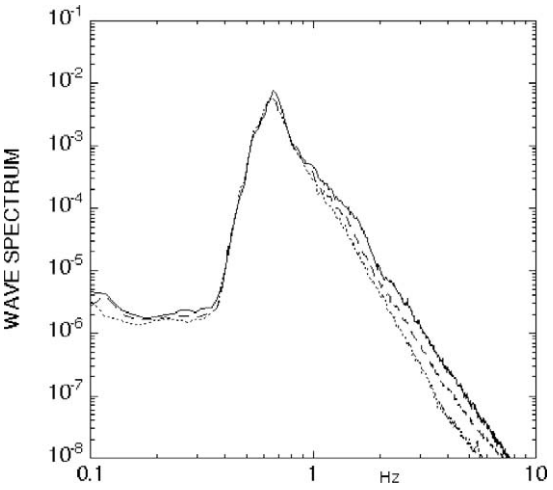

Fig. 7. Wave spectra for BFI = 0.9 at $x/L = 2.8$ (solid line), $x/L = 21.2$ (dashed line) and $x/L = 56.9$ (dotted line).

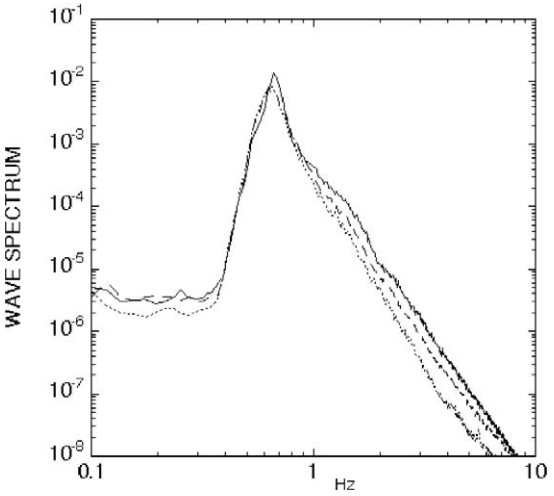

Fig. 8. Wave spectra for BFI = 1.2 at $x/L = 2.8$ (solid line), $x/L = 21.2$ (dashed line) and $x/L = 56.9$ (dotted line).

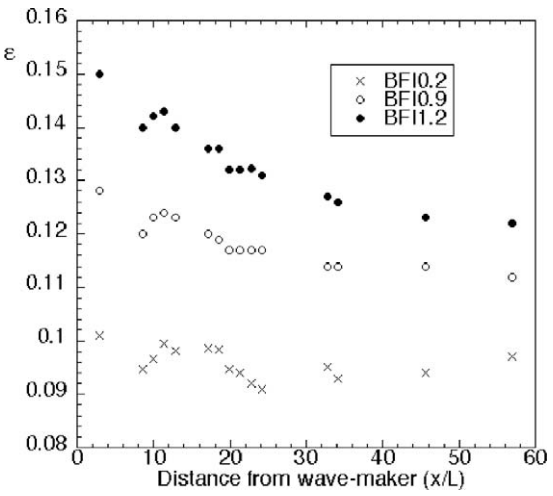

Fig. 9. Wave steepness as a function of nondimensional fetch.

also observed. We now define from the experimental time series the density of rogue waves as the number of wave heights, considering both zero up-crossing and down-crossing waves, that satisfies the condition $H \geqslant 2H_s$ over the total number of wave heights recorded. In Fig. 10 we show the rogue wave density at different distances from the wave maker. Up to around 15 wavelengths from the wave maker the rogue wave density is bounded between 10^{-4} and 1.2×10^{-3}. While the density for BFI = 0.2 remains more or less at the same level, the rogue wave density increases substantially for BFI = 0.9 and BFI = 1.2 reaching a maximum of 3.1×10^{-3} for BFI = 1.2. Then in the last part of the tank the number of rogue waves decreases. This result is consistent with the analysis of the kurtosis described in [32]. According to our expectations, the number of rogue waves recorded increases as the Benjamin–Feir index of the initial condition increases. Note also that according to the second order theory (which will be discussed in the next section) the nonlinearity depends on the wave steepness (and not on the BFI). In the present case the wave steepness decreases along the tank, while the rogue wave density increases and reaches a maximum after about 25 wavelengths; therefore the increase of the rogue wave density cannot be attributed only to the second order corrections.

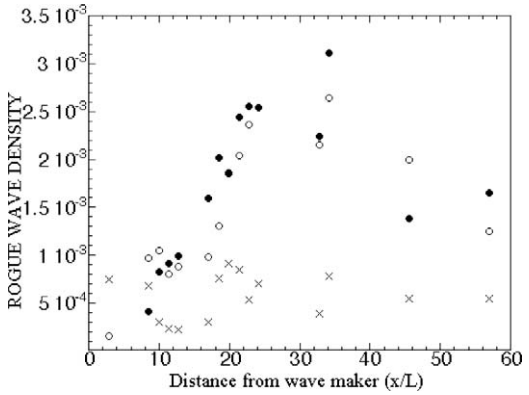

Fig. 10. Rogue wave density for BFI = 0.2, crosses; BFI = 0.9, empty circles; BFI = 1.2, full circles (see Table 1).

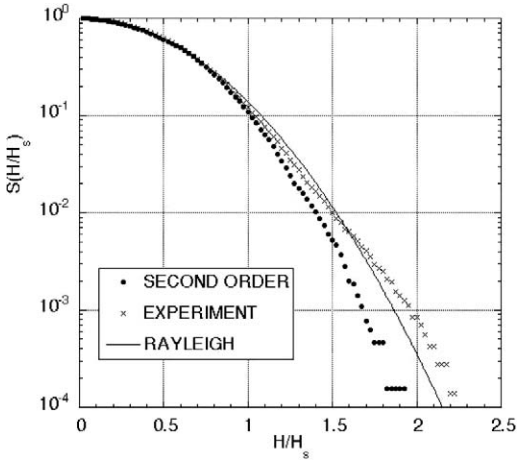

Fig. 11. Wave height survival function at $x/L = 2.8$ for BFI = 0.2. Solid line corresponds to the Rayleigh distribution, crosses are experimental data and circles are the results of second order theory.

4.3. Wave height and wave crest distributions: a comparison with the second order theory

The second order theory has been derived from the Euler equations as a superposition of linear traveling wave solutions with random phases corrected to second order. The wave spectrum does not change in time as the wave field evolves. Therefore, the solution of the problem does not include any nonlinear dynamics of free waves (and of course the modulational instability). The theory is developed for arbitrary depth and is valid for any directional spreading. According to the second order theory, time series of the surface elevation for infinite-crested waves, in infinite water depth, can be built up in the following way (see [40]):

$$\eta(t) = \sum_{i=1}^{N} a_i \cos(-\omega_i t + \phi_i) + \frac{1}{4}\sum_{i=1}^{N}\sum_{j=1}^{N} a_i a_j \left[K^- \cos\left[-(\omega_i - \omega_j)t + \phi_i - \phi_j\right] + K^+ \cos\left[-(\omega_i + \omega_j)t + \phi_i + \phi_j\right]\right] \tag{7}$$

a_i is related to the wave spectrum as $a_i = \sqrt{2P(f)\Delta f}$, with $P(f)$ the spectral density function of the surface elevation and Δf the spectral resolution; ϕ_i are random phases. The coupling coefficients K^+ and K^- for infinite water depth are given in [40]. The time series of the surface elevation obtained with Eq. (7) is then processed as an experimental time series to obtain the wave height distribution.

Some results on the survival function for wave heights for the same experimental data have been presented in [31]. Here we compare the survival function for wave heights and wave crests with the Rayleigh distribution and with the one obtained from second order theory. We expect that for wave heights the second order theory should not have any effect on the distribution and it should be very close to the Rayleigh distribution (Eq. (1)).

In Fig. 11 we show the survival function for BFI = 0.2 at the first probe for $x/L = 2.8$. In the same figure we also show the Rayleigh distribution and the distribution obtained from analysis of the time series generated with Eq. (7). We recall that the wave field has been generated at the wave maker as a linear superposition of random waves. Figs. 12, 13 show the same kind of plot as in 11 at different distances from the wave maker (respectively at $x/L = 21.3$ and $x/L = 45.5$). These three plots (Figs. 11–13) show that for the present case (BFI = 0.2) the Rayleigh distribution describes reasonably well the experimental data up to the probability of 10^{-3}; some deviations still observed for higher probability level. The second order theory underestimates the Rayleigh distribution (and of course our experimental data); this is consistent with many observations (see [7] and comments in [8]).

In Figs. 14–19 we show the survival function for BFI = 0.9 and BFI = 1.2. In both cases we see that at the first probe $x/L = 2.8$ (Figs. 14 and 17) the Rayleigh distribution overestimates slightly our experimental results (and

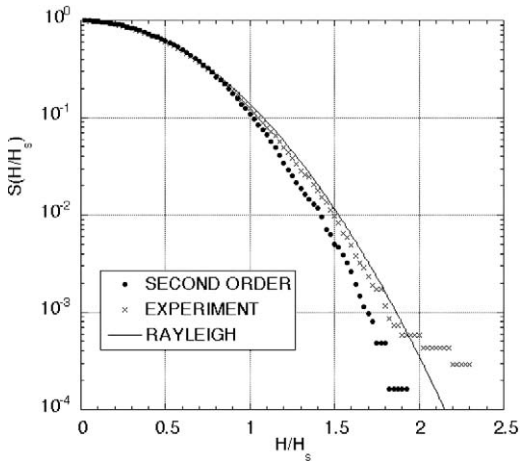

Fig. 12. Wave height survival function at $x/L = 21.3$ for BFI $= 0.2$. Solid line corresponds to the Rayleigh distribution, crosses are experimental data and circles are the results of second order theory.

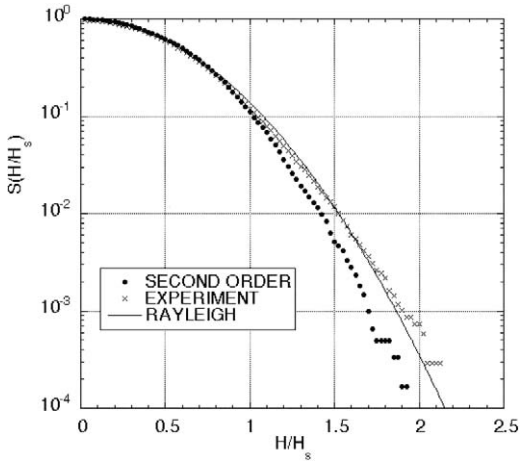

Fig. 13. Wave height survival function at $x/L = 45.5$ for BFI $= 0.2$. Solid line corresponds to the Rayleigh distribution, crosses are experimental data and circles are the results of second order theory.

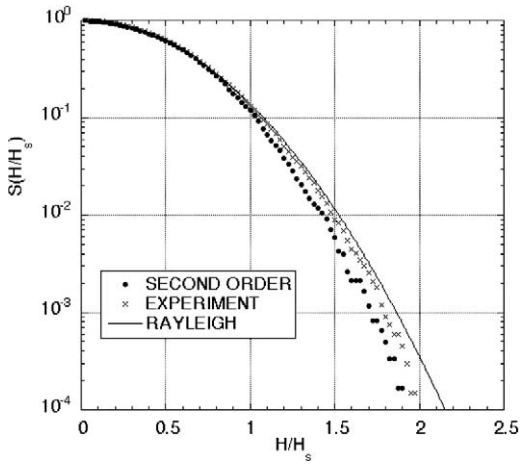

Fig. 14. Wave height survival function at $x/L = 2.8$ for BFI $= 0.9$. Solid line corresponds to the Rayleigh distribution, crosses are experimental data and circles are the results of second order theory.

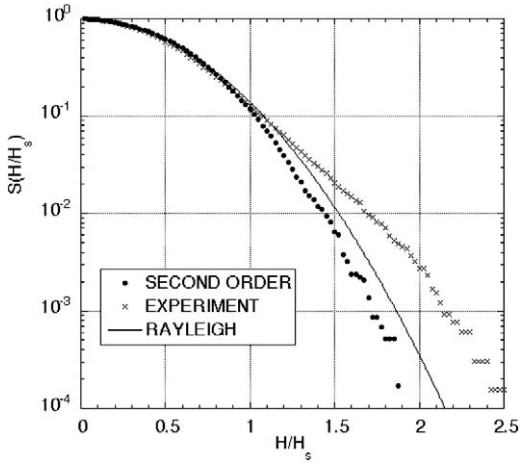

Fig. 15. Wave height survival function at $x/L = 21.3$ for BFI $= 0.9$. Solid line corresponds to the Rayleigh distribution, crosses are experimental data and circles are the results of second order theory.

second order results too). We recall that the nonlinear interactions among free waves, responsible for the modulational instability, needs some space to take place (see also Fig. 10 where it is clear that the nonlinearity takes some wave lengths to develop). Figs. 15, 16 and 18, 19 show clearly that the experimental data start departing from the Rayleigh distribution at a probability level of 10^{-1}. In Fig. 20 we compare our experimental results with Fig. 6(b) in [18] that has been obtained by numerical simulations of the Dysthe equation, using as initial condition a Jonswap spectrum with $\alpha = 0.0081$ and $\gamma = 6$ (see [18] for details). The Benjamin–Feir index calculated for this spectrum has approximately the value BFI $= 0.9$, therefore the probability distribution from numerical simulations can be compared with our experimental data with the same BFI. The agreement is quite good.

We now consider the survival function for wave crests. For wave crests distribution, the second order theory should play a major role, therefore the reference distribution against which we will compare our experimental data is not anymore the Rayleigh but the Tayfun distribution (Eq. (2)). In Figs. 21–23 we show the experimental wave crest distributions for the run BFI $= 0.2$ compared with data from second order theory and Tayfun distribution (wave crests are normalized with the standard deviation of the surface elevation σ). While these last two distributions are quite in

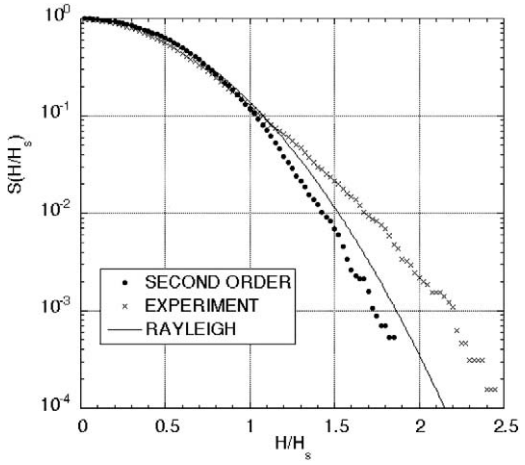

Fig. 16. Wave height survival function at $x/L = 45.5$ for BFI = 0.9. Solid line corresponds to the Rayleigh distribution, crosses are experimental data and circles are the results of second order theory.

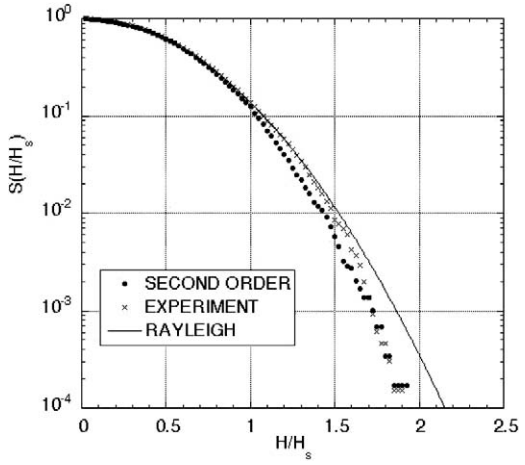

Fig. 17. Wave height survival function at $x/L = 2.8$ for BFI = 1.2. Solid line corresponds to the Rayleigh distribution, crosses are experimental data and circles are the results of second order theory.

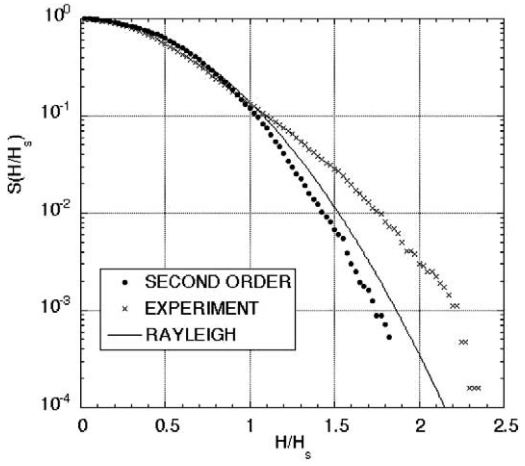

Fig. 18. Wave height survival function at $x/L = 21.3$ for BFI = 1.2. Solid line corresponds to the Rayleigh distribution, crosses are experimental data and circles are the results of second order theory.

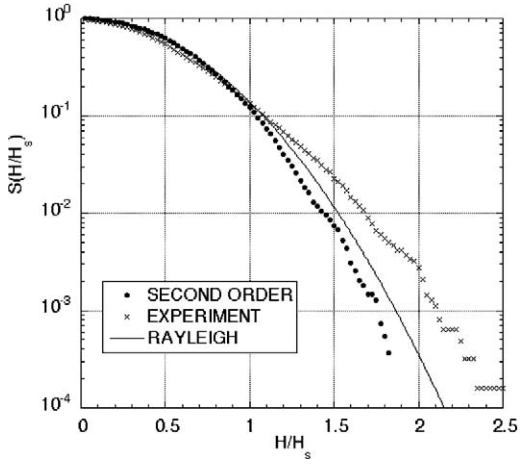

Fig. 19. Wave height survival function at $x/L = 45.5$ for BFI = 1.2. Solid line corresponds to the Rayleigh distribution, crosses are experimental data and circles are the results of second order theory.

agreement, the experimental curve shows, especially for $x/L = 2.8$ and $x/L = 21.3$ (Figs. 22, 23) departures from these distributions. For larger BFI (BFI = 0.9 and BFI = 1.2) the departure is more pronounced (Figs. 24–27) as the distance from the wave maker is increased. This is again consistent with the fact that the nonlinear interactions need some space to manifest themselves. It is interesting to note that departures from theory are observed starting from a probability of 10^{-1}. Moreover, it is clear for example from Figs. 25, 26 and 28, 29 that the theoretical predictions underestimate the experimental curve by more than one order of magnitude.

5. Discussion and conclusions

Recently a large number of papers have appeared that suggest that the modulational instability is a possible mechanism for explaining the formation of freak waves. A pioneering work in this context was performed by Trulsen and Dysthe [13], who for the first time considered seriously the possibility of describing nonlinear extreme waves using envelope equations. This work was also supported by a number of numerical and theoretical papers in which particular

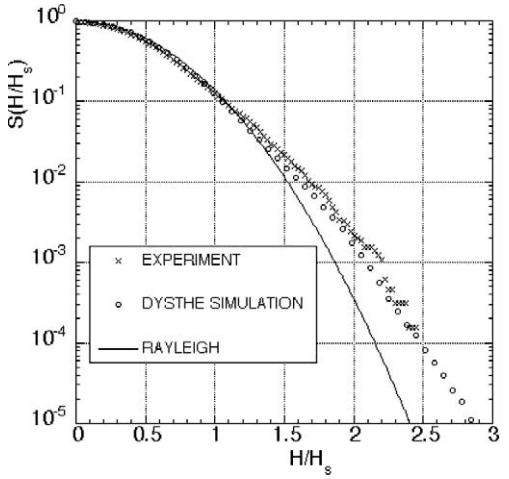

Fig. 20. Comparison of experimental results at $x/L = 32.7$ with results from numerical simulation of the Dysthe equation, see [18] for details of the numerical simulations.

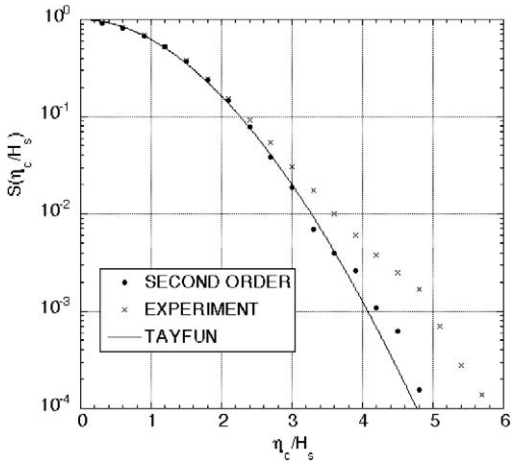

Fig. 21. Wave crest survival function at $x/L = 2.8$ for BFI $= 0.2$. Solid line corresponds to the Tayfun distribution, crosses are experimental data and dots are the results of second order theory.

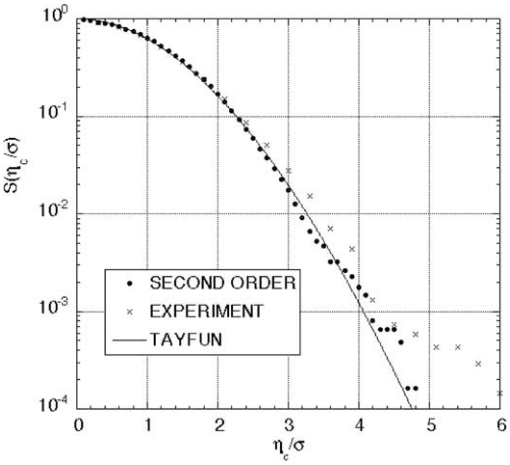

Fig. 22. Wave crest survival function at $x/L = 21.3$ for BFI $= 0.2$. Solid line corresponds to the Tayfun distribution, crosses are experimental data and dots are the results of second order theory.

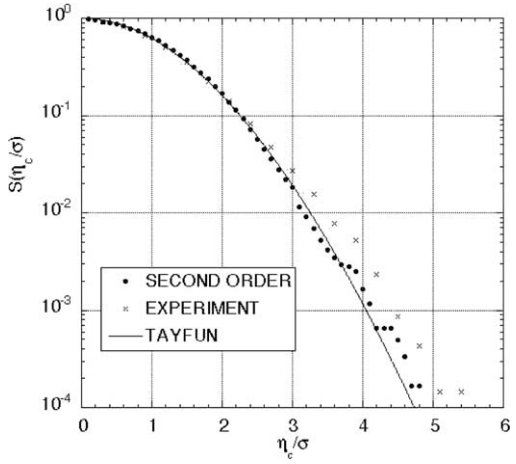

Fig. 23. Wave crest survival function at $x/L = 45.5$ for BFI $= 0.2$. Solid line corresponds to the Tayfun distribution, crosses are experimental data and dots are the results of second order theory.

analytical solutions (see [41]) of the NLS equations were considered as candidates for rogue waves [25,26,42]. An important result obtained from numerical simulations is that these "breather" solutions are very robust and can be excited also from random spectra [24]. Their dynamics is quite different from the rest of the random wave field, they survive after interactions with other waves and periodically appear as large amplitude waves, while disappearing after some wavelengths. If the random wave field is very nonlinear (large steepness and small spectral width, corresponding to large BFI), the density of these objects increases, each of them having its own unique dynamics. Starting from an initial random wave field, they need several wavelengths (in our case about 25–30 wavelengths) to emerge from the background wave field. In a nonlinear wave field their presence is statistically significant, clearly leaving their signature in the survival function of wave heights. This phenomenological description is consistent with our experimental data. For the NLS equation these objects survive forever in an ideal simulation; indeed it can be shown that they correspond to proper modes, called unstable modes, of the NLS equation and therefore correspond to constants of the motion, as for example solitons can be considered as constant of motion for the Korteweg de Vries equation.

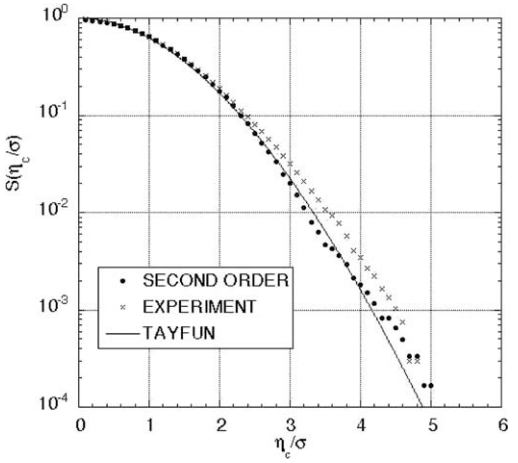

Fig. 24. Wave crest survival function at $x/L = 2.8$ for BFI $= 0.9$. Solid line corresponds to the Tayfun distribution, crosses are experimental data and dots are the results of second order theory.

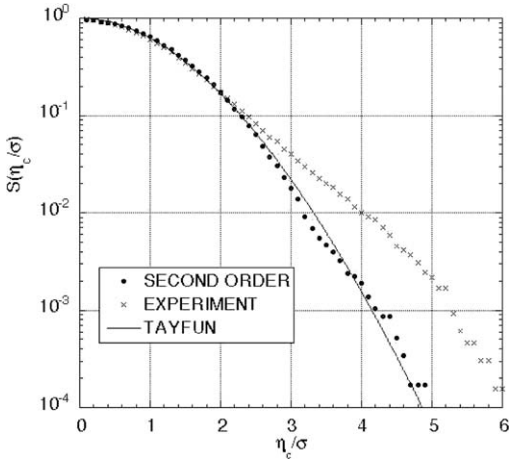

Fig. 25. Wave crest survival function at $x/L = 21.3$ for BFI $= 0.9$. Solid line corresponds to the Tayfun distribution, crosses are experimental data and dots are the results of second order theory.

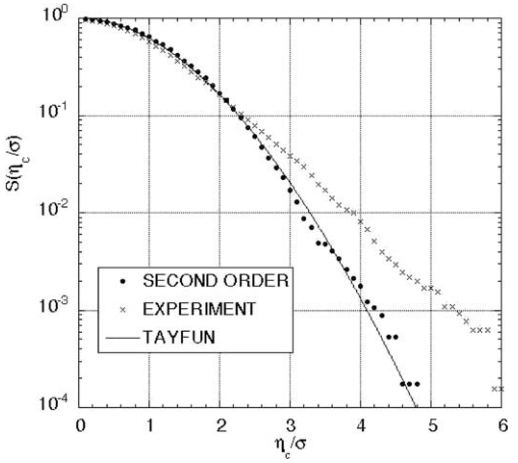

Fig. 26. Wave crest survival function at $x/L = 45.5$ for BFI $= 0.9$. Solid line corresponds to the Tayfun distribution, crosses are experimental data and dots are the results of second order theory.

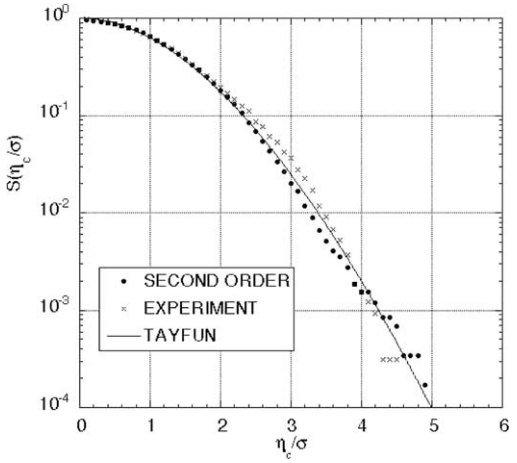

Fig. 27. Wave crest survival function at $x/L = 2.8$ for BFI $= 1.2$. Solid line corresponds to the Tayfun distribution, crosses are experimental data and circles are the results of second order theory.

The experiments performed at Marintek support this picture. Indeed we have shown that the number of rogue waves (which in the language of the NLS equation roughly corresponds to the number of unstable modes) depends on the Benjamin–Feir index of the initial spectrum. The presence of these modes determines the shape of the probability density function of wave heights. For nonlinearities consistent with water waves, the density of these modes is not very large, 3×10^{-3}, therefore a large number of waves should be recorded in order to have reliable statistics. Even if we have collected a large number of data, sufficient to observe a clear departure from the Rayleigh and Tayfun distributions, we believe that statistics computed on even larger data sets should be used in order to model the tail of the survival function. For large values of the BFI we have also observed a change of the spectrum on the same scale as variations the modulational instability. This result is consistent with recent numerical simulations in [5]. According to their simulations, the theoretical work by Janssen and the present experimental results, changes in the spectrum can be observed on a time scale of $1/(\omega_0\epsilon^2)$. Theoretically this result is attributed to the so called quasi-resonant interactions (see [15]). The Benjamin–Feir instability is an example of this kind of interaction. Whether these interactions are frequent in the real ocean is still an open question and some effort should be focused to answer this question.

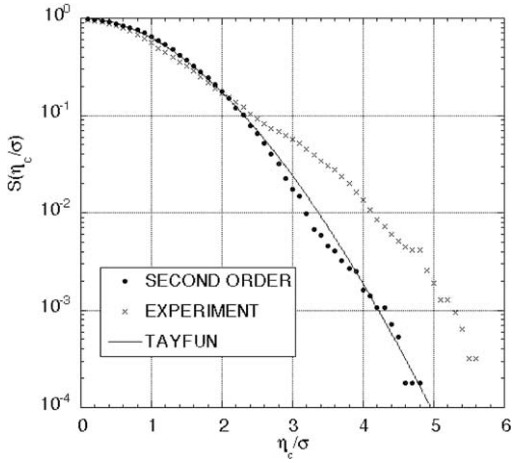

Fig. 28. Wave crest survival function at $x/L = 21.3$ for BFI = 1.2 Solid line corresponds to the Tayfun distribution, crosses are experimental data and circles are the results of second order theory.

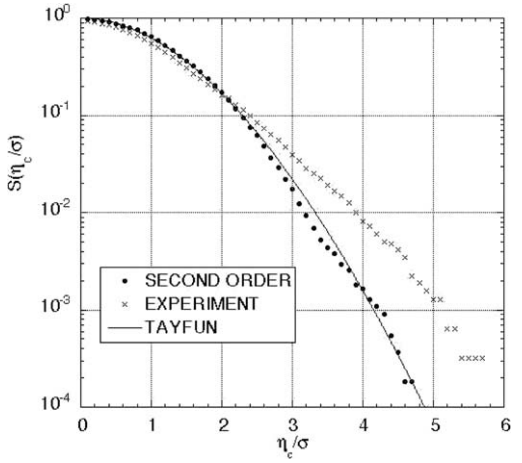

Fig. 29. Wave crest survival function at $x/L = 45.5$ for BFI = 1.2. Solid line corresponds to the Tayfun distribution, crosses are experimental data and circles are the results of second order theory.

We feel that our results are definitely important for researchers who perform experiments in wave flumes, especially when studying the interactions of waves with structures where the usual approach is to run a Jonswap spectrum and to assume that wave heights are Rayleigh distributed.

One of the limits of our work is that our experiment has been performed in the case of infinite crested waves. For directionally spread propagation, numerical and experimental work on the probability density function of wave heights is more difficult because numerics becomes much more expensive and experimental work requires large basins with wave makers capable of generating waves in different directions. So far, on the specific problem of the relevance of the modulational instability in $2+1$ dimensions, only a few numerical results are available [44,5,43]. In [44], using the Dysthe equation in $2+1$ dimensions with the exact linear dispersion relation, it was shown that, if the directional spreading is sufficiently narrow, the kurtosis of the surface elevation reaches values larger than 3 (the value for Gaussian distribution); for larger directional spreadings, the kurtosis oscillates around the Gaussian value. This result is consistent with experimental work carried out in the Ocean Basin at Marintek [45]. In [5], the authors performed numerical simulations of the $2+1$ Dysthe equation with three different spectra as initial conditions characterized by different directional spreading. For the case of long crested waves, their result, as previously mentioned, is consistent with our experimental results; for large directional spreadings they show that the Tayfun distribution is very close to their numerical data. It should be stated that in $2+1$ dimensions, standard four wave resonant interactions tend to broaden irreversibly the spectrum and generate a tail of the form of ω^{-4} [39,46]. Therefore the instability may take place only at the very initial stages of a freely decaying simulation. Definitely more results including wind forcing and dissipation in $2+1$ dimensions are needed for determining the role of the modulational instability for wind waves in realistic conditions.

Appendix A

Here we report the coefficients of the nonlinear and dispersive term of the NLS equation written in arbitrary depth:

$$\sigma = 2 - \nu^2 + 8(k_0h)^2 \frac{\cosh(2k_0h)}{\sinh^2(2k_0h)}, \tag{8}$$

$$\beta = \frac{8 + \cosh(4k_0h) - 2\tanh^2(k_0h)}{8\sinh^4(k_0h)} - \frac{(2\cosh^2(k_0h) + 0.5\nu)^2}{\sinh^2(2k_0h)(k_0h/\tanh(k_0h) - \nu^2/4)} \tag{9}$$

with

$$\nu = 1 + 2\frac{k_0h}{\sinh(2k_0h)}. \tag{10}$$

Acknowledgements

We thank P. Janssen and K. Trulsen for valuable discussions. Froydis Solaas is also acknowledged for technical support during the experiment. This research has been supported by the Improving Human Potential – Transnational Access to Research Infrastructures Programme of the European Commission under the contract HPRI-CT-2001-00176. M.O., A.O. and M.S. have also been supported by the Ministero dell'Istruzione, dell'Università e della Ricerca.

References

[1] S.O. Rice, Mathematical analysis of random noise, in: N. Wax (Ed.), Noise and Stochastic Processes, Dover Publications, New York, 1954, pp. 133–294.
[2] M.S. Longuet-Higgins, On the statistical distribution of the heights of sea waves, J. Marine Res. 11 (1952) 1245–1266.
[3] M.S. Longuet-Higgins, The effect of non-linearities on statistical distributions in the theory of sea waves, J. Fluid Mech. 17 (1963) 459–480.
[4] M.A. Tayfun, Narrow–band nonlinear sea waves, J. Geophys. Res. 85 (1980) 1548–1552.
[5] H. Socquet-Juglard, K. Dysthge, K. Trulsen, H.E. Krogstad, J. Liu, Distribution of surface gravity waves during spectral changes, J. Fluid Mech. 542 (2005) 195–216.
[6] M.D. Earle, Extreme wave conditions during Hurricane Camille, J. Geophys. Res. 80 (1975) 377–379.
[7] G.Z. Forristall, On the statistical distribution of wave heights in a storm, J. Geophys. Res. 83 (1978) 2553–2558.
[8] M.S. Longuet-Higgins, On the distribution of the heights of sea waves: Some effects of nonlinearity and finite band width, J. Geophys. Res. 85 (1980) 1519–1523.
[9] A. Naess, On the statistical distribution of crest to trough wave heights, Ocean Engrg. 12 (1985) 221–234.
[10] I.V. Lavrenov, The wave energy concentration at the Agulhas current of South Africa, Natural Hazards 17 (1998) 117–127.
[11] B.S. White, B. Fornberg, On the chance of freak waves at the sea, J. Fluid Mech. 255 (1998) 113–138.
[12] K.L. Henderson, D.H. Peregrine, J.W. Dold, Unsteady water wave modulations: fully nonlinear solutions and comparison with the nonlinear Schrödinger equation, Wave Motion 29 (1999) 341–361.
[13] K. Trulsen, K.B. Dysthe, Freak waves – a three-dimensional wave simulation, in: Proceedings of the 21st Symposium on Naval Hydrodynamics, National Academy Press, Washington, DC, 1997, pp. 550–560.
[14] C. Kharif, E. Pelinovsky, Physical mechanisms of the rogue wave phenomenon, Eur. J. Mech. B Fluids 22 (2003) 603–634.
[15] P.A.E.M. Janssen, Nonlinear four-wave interactions and freak waves, J. Phys. Ocean. 33 (2003) 863–883.
[16] N. Mori, Occurrence probability of freak wave in nonlinear wave field, Ocean Engrg. 31 (2004) 165–175.
[17] N. Mori, P.A.E.M. Janssen, On kurtosis and occurrence probability of freak waves J. Phys. Ocean. (2006), in press.
[18] M. Onorato, A.R. Osborne, M. Serio, T. Damiani, Occurrence of freak waves from envelope equations in random ocean wave simulations, M. Olagnon, G.A. Athanassoulis (Eds.), Rogue Wave 2000, Ifremer, Brest, 29–30 November 2000, 181–192.
[19] N. Mori, T. Yasuda, Effects of higher-order nonlinear wave-wave interactions on deep-water waves, M. Olagnon, G.A. Athanassoulis (Eds.), Rogue Wave 2000, Ifremer, Brest, 29–30 November 2000, 229–244.
[20] C. Brandini, Nonlinear interaction processes in extreme wave dynamics, Tesi di Dottorato, Università di Firenze, 2001.
[21] D.G. Dommermuth, D.K.P. Yue, A high-order spectral method for the study of nonlinear gravity waves, J. Fluid Mech. 184 (1987) 267–288.
[22] I.E. Alber, The effects of randomness on the stability of two dimensional surface wave trains, Proc. Roy. Soc. London Ser. A 636 (1978) 525–546.
[23] P.A.E.M. Janssen, On nonlinear wave groups and consequences for spectral evolution, in: R.C. Beal (Ed.), Directional Ocean Wave Spectra, The Johns Hopkins University Press, 1991, pp. 46–52.
[24] M. Onorato, A.R. Osborne, R. Fedele, M. Serio, Landau damping and coherent structures in narrow-banded $1 + 1$ deep water gravity waves, Phys. Rev. E 67 (2003) 046305.
[25] K.B. Dysthe, K. Trulsen, Note on breather type solutions of the NLS as a model for freak waves, Phys. Scripta T 82 (1999) 48–52.
[26] A.R. Osborne, M. Onorato, M. Serio, The nonlinear dynamics of rogue waves and holes in deep-water gravity wave trains, Phys. Lett. A 275 (2000) 386–393.
[27] M. Onorato, A.R. Osborne, S. Bertone, Freak waves in random oceanic sea states, Phys. Rev. Lett. 86 (2001) 5831–5834.
[28] C.T. Stansberg, Nonlinear extreme wave evolution in random wave groups, in: International Society of Offshore and Polar Engineers, Seattle, USA, May 28–June 2, 2000, 2000, pp. 1–8.
[29] C.T. Stansberg, On spectral instabilities and development of nonlinearities in propagating deep-water wave trains, in: Coastal Engineering, Proceedings of the XXIII International Conference, Venice, Italy, October 4–9, 1992, pp. 658–671.
[30] N.E. Huang, S.R. Long, An experimental study of the surface elevation probability distribution and statistics of wind-generated waves, J. Fluid Mech. 101 (1980) 179–200.
[31] M. Onorato, R. Osborne, M. Serio, C. Brandini, C.T. Stansberg, Observation of strongly non-Gaussian statistics for random sea surface gravity waves in wave flume experiments, Phys. Rev. E 70 (2004) 067302.
[32] M. Onorato, R. Osborne, M. Serio, L. Cavaleri, Modulational instability and non-Gaussian statistics in experimental random water-wave trains, Phys. Fluids 17 (2005) 078101.
[33] V. Zakharov, Stability of periodic waves of finite amplitude on the surface of a deep fluid, J. Appl. Mech. Tech. Phys. 9 (1968) 190–194.
[34] C.C. Mei, The Applied Dynamics of Ocean Surface Waves, John Wiley, New York, 2000.
[35] G.J. Komen, L. Cavaleri, M. Donelan, K. Hasselmann, H. Hasselmann, P.A.E.M. Janssen, Dynamics and Modeling of Ocean Waves, Cambridge University Press, 1994.

[36] N.E. Huang, C.C. Tung, S.R. Long, Wave spectra, The Sea: Ocean Engrg. Sci. 9 (1990) 197–237.
[37] M. Serio, M. Onorato, A.R. Osborne, P.A.E.M. Janssen, On the computation of the Benjamin–Feir index, Nuovo Cimento C 28 (2005) 893–903.
[38] C.T. Stansberg, Propagation-dependent spatial variations observed in wave trains generated in a long wave tank, Data Report 490030.01 Marintek, Sintef group, Trondheim, 1993.
[39] K.B. Dysthe, K. Trulsen, H.E. Krogstad, H. Socquet-Juglard, Evolution of a narrow-band spectrum of random surface gravity waves, J. Fluid Mech. 478 (2003) 1–10.
[40] G.Z. Forristall, Wave crest distributions: Observations and second-order theory, J. Phys. Ocean. 30 (2000) 1931–1943.
[41] N.N. Akhmediev, A. Ankiewicz, Solitons, Nonlinear Pulses and Beams, first ed., Optical and Quantum Electronic Series, vol. 5, Chapman and Hall, 1997.
[42] D.H. Peregrine, Water waves, nonlinear Schrödinger equations and their solutions, J. Austral. Math. Soc. B 25 (1983) 16–43.
[43] A. Slunyaev, C. Kharif, E. Pelinovsky, T. Talipova, Nonlinear wave focusing on water of finite depth, Physica D 173 (2002) 77–96.
[44] M. Onorato, A.R. Osborne, M. Serio, Extreme wave events in directional, random oceanic sea states, Phys. Fluids 14 (2002) L25–L28.
[45] C.T. Stansberg, Effects from directionality and spectral bandwidth on nonlinear spatial modulations of deep water surface gravity wave trains, in: Coastal Engineering, Proceedings of the XXIV International Conference, Kobe, Japan, October 23–28, 1994, pp. 579–593.
[46] M. Onorato, A.R. Osborne, M. Serio, D. Resio, A. Pushkarev, V.E. Zakharov, C. Brandini, Freely decaying weak turbulence for sea surface gravity waves, Phys. Rev. Lett. 89 (2002) 144501.